Electrodeposited Zinc Anodes On Nickel Foam For Enhanced Zinc-Air Battery Performance

Chen Shunhong, Teerasak Hudakorn, and Saroj Pullteap*

Department of Mechanical Engineering, Faculty of Engineering and Industrial Technology, Silpakorn University, Nakhon Pathom, Thailand

* *Corresponding author. E-mail: saroj@su.ac.th*

Received: Aug. 10, 2025; Accepted: Oct. 1, 2025

The uneven deposition of zinc on the electrode surface leads to inadequate durability and stability of zinc-air batteries, hindering their widespread application. This study systematically investigates the fabrication of zinc anodes by electrochemical deposition onto nickel foam substrates and evaluates their performance in zinc-air batteries. Zinc was deposited for varying durations ($3-5$ hours), and the resulting electrodes were characterized using Scanning Electron Microscopy coupled with Energy-Dispersive X-ray Spectroscopy (SEMEDS), X-ray Diffraction (XRD), X-ray Photoelectron Spectroscopy (XPS) and Transmission Electron Microscopy (TEM). Electrochemical measurements show that the sample deposited for 4 hours delivers the best overall performance, with an average discharge voltage of 1.17 V and a load current of 3.52 mA which is 21% higher than cells with pure- Zn anodes. Microstructural analysis further confirms that 4 hours affords the optimal balance between zinc loading (84.01wt%) and deposition uniformity. This study delineates the structureperformance correlation among electrodeposition time, zinc loading, microstructural features, and electrochemical behavior, offering vital theoretical guidance and process reference for the optimized fabrication of metal-air battery anodes.

Keywords: Zinc anode; electrochemical deposition; nickel foam; zinc-air battery

http://dx.doi.org/10.6180/jase.202605_29(5).0019

1. Introduction

With the continuous growth of global energy demand and the escalating severity of environmental issues, the massive consumption of fossil fuels has led to serious greenhouse effects and environmental pollution, making the development of clean energy a key pathway to address these problems [1–3]. However, the inherent intermittency and unpredictability of clean renewable energies such as solar and wind power severely hinder their large-scale application; therefore, the development of efficient and reliable energy storage systems is urgently needed [4, 5]. Among various energy storage technologies, lithium-ion batteries dominate the market, yet their energy density is limited (< 350 Wh kg^{-1}), the cost remains relatively high (about 150USD kW h^{-1}), and potential safety risks have not been fundamentally resolved [6–10]. In contrast, zinc-based batteries are regarded as highly promising nextgeneration energy storage technologies due to their high theoretical energy density, low cost, and intrinsic safety [11–13].

As the anode material in the first voltaic cell invented by Alessandro Volta, zinc has shown great potential in the history of secondary battery development and continues to attract research attention [14–16]. Zinc is abundant and environmentally friendly, possesses a high theoretical capacity (820mAh g^{-1}), and exhibits a relatively low hydrogen evolution overpotential in aqueous electrolytes, making it an ideal choice for constructing safe and low-cost energy storage systems [17–21]. In commercial applications, zinc has been successfully used in alkaline nickel-zinc batter-

ies to replace precious metal hydrides, or combined with air cathodes to achieve practical specific energies up to 400 Wh kg^{-1} [13, 22–26]. However, current zincbased batteries, such as alkaline zinc-nickel and zinc-manganese cells, require high areal capacity and deep discharge depth (DoD) to compete with lithium-ion batteries. Due to limited electrolyte volume, these batteries struggle to maintain long-term stable operation [13, 27]. Among zinc-based batteries, zinc-air batteries have garnered particular attention for their unique performance advantages and ultra-high theoretical energy density (1, 353 Wh kg^{-1}, excluding oxygen mass). Despite their high theoretical energy density, the practical energy density and cycle life of zinc-air batteries remain limited. This is mainly owing to dendrite growth and morphological deformation of the zinc anode, as well as performance degradation of the air cathode [7]. Failure of the air electrode is closely related to the loss of active area, electrode flooding, catalyst deactivation, and pore blockage [28]. Therefore, developing highperformance zinc anodes (e.g., suppressing dendrite growth and improving electrochemical reversibility) is one of the core challenges to promote the commercial application of zinc-air batteries [29–32].

This study focuses on optimization strategies for zinc-air battery anodes by electrochemically depositing zinc onto nickel foam substrates, aiming to enlarge the anode reaction area and optimize the microstructure, thereby significantly enhancing the overall performance of the zinc-air battery. We employed advanced techniques, including X-ray diffraction (XRD), scanning electron microscopy (SEM), transmission electron microscopy (TEM), X-ray photoelectron spectroscopy (XPS), and electrochemical impedance spectroscopy (EIS), to systematically evaluate the effects of the electrochemical deposition process and its impact on battery performance. This work provides important experimental data and theoretical guidance for the design and fabrication of efficient and stable metal-air battery anode materials.

2. Materials and methods

2.1. Materials

All commercially available reagents were of analytical grade and used as received without further purification. Deionized water (resistivity $>$ 18.2M$\Omega \cdot$ cm) was used throughout the experiments. Commercial nickel foam (thickness 1.5 mm , pore density 100 PPI , Kunshan Xingzhenghong Battery Materials Co., Ltd.) was used as the substrate. All experiments were conducted at room temperature.

2.2. Pretreatment of Nickel Foam Substrate

Commercial nickel foam was cut to the required size (35 $\times$ 60 mm) and subjected to the following surface treatment steps: First, the samples were immersed in a mixed solution of hydrochloric acid (35wt%) and deionized water at a volume ratio of 1 : 2 and ultrasonically cleaned for 15 min to remove surface oxides and impurities. Subsequently, the samples were rinsed sequentially in three deionized water baths (5 min for each) to remove residual acid and ultrasonically in anhydrous ethanol (99.8% purity) for 15 minutes to remove organic contaminants. Finally, the pretreated substrates were dried in an oven at 60°C for 12 hours and the mass change was recorded using a precision balance.

2.3. Electrochemical Deposition of Zinc Anode

A CS350 electrochemical workstation (Wuhan Corrtest Instrument Co., Ltd) was used to electrodeposit zinc particles onto the three-dimensional porous nickel foam substrate via chronopotentiometry (CP). An aqueous solution of 0.5 mol L^{-1} zinc sulfate heptahydrate ($ZnSO_4 \cdot 7H_2O$, analytical grade, purity $\geq$ 98.5%) served as the electrolyte in a two-electrode configuration: nickel foam as the working electrode and pure zinc as the counter electrode. Electrodeposition was carried out at a constant current density of 0.11 A cm^{-2} using the electrochemical workstation.

To maintain uniform ionic concentration in the electrolyte and effectively remove bubbles generated at the electrode interface, magnetic stirring at 60 rpm was applied throughout the experiment. Deposition times were set to 3 hours, 4 hours, and 5 hours, with the corresponding samples designated as Zn3, Zn4, and Zn5 , respectively. Six parallel samples were prepared for each condition to ensure statistical reliability of the data. After electrodeposition, the samples were rinsed with deionized water and then dried at 60°C for 12 hours in a vacuum oven to obtain composite electrodes with uniform zinc coatings. The deposition efficiency was calculated gravimetrically, and the results showed an average efficiency of 89 $\pm$ 3%.

2.4. Assembly of Zinc-Air Batteries

The Zn3, Zn4, Zn5 were used as the anodes, and a high-surface area carbon plate (10 $\times$ 60 mm, 99% purity) loaded with platinum catalyst was used as the air cathodes. KOH aqueous solution (A 6 mol L^{-1}) served as the electrolyte, and a glass fiber filter (GF/C, 47 mm diameter) which is prewetted with electrolyte was employed as the separator. The cell housing consisted of three custom acrylic plates (60 $\times$ 70 $\times$ 15 mm) with 0.5 mm -thick silicone gaskets to ensure good sealing. The assembled batteries were designated

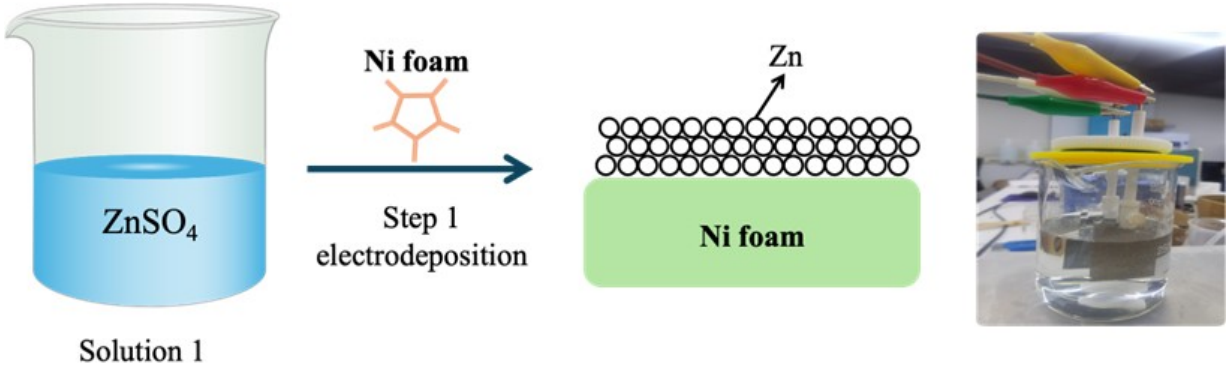

Fig. 1. Schematic illustration of electrodeposition process of zinc on nickel foam

Zn3 B, Zn4 B, and Zn5 B , respectively. Meanwhile, a pure zinc plate (35×60 mm, 2 mm thick) was used as a control anode, with all other components unchanged, to assemble a standard zinc-air battery for comparison, designated StZnB . After assembly, all batteries were allowed to stand for 10 min to ensure full electrolyte infiltration and stabilization of the electrode/electrolyte interface before performance testing.

2.5. Physical Characterization and Electrochemical Performance Testing

The phase composition and crystal structure of the zinc coating were characterized by X ray diffraction (XRD, Rigaku Ultima IV) using Cu Kα radiation ($\lambda = 1.5406$ Å), with a scanning range of $5^\circ - 80^\circ$ and a scan rate of 8°/min. A scanning electron microscope (SEM, Thermo Scientific Apreo2) equipped with an energy-dispersive X-ray spectrometer (EDS) and a transmission electron microscope (TEM, Talos F200S) were used to examine the micromorphology and elemental distribution of the zinc coating, operated at 5 kV accelerating voltage and 50 pA beam current. X-ray photoelectron spectroscopy (XPS, Thermo Scientific K-Alpha) was employed to analyze the valence states of surface elements, with all binding energies calibrated to the C 1s peak (adventitious carbon on the sample surface) at 284.8 eV . Electrochemical performance was evaluated using a digital multimeter and a data acquisition system to measure the open-circuit voltage, load voltage, and load current of both the control cell with a pure zinc plate anode and the zinc-plated nickel foam anode cells. Voltage decay and current fluctuations were continuously recorded over 6 hours, with a light-emitting diode (LED) serving as the external load.

3. Results and discussion

3.1. Physical Characterization

To provide a clear understanding of the experimental methodology and to visually present the basic preparation process of the zinc anode, a schematic diagram of the electrochemical deposition process is shown in Fig. 1. This diagram offers the necessary background for the system approach used in this study. Uniform zinc-coated nickel foam composites were successfully fabricated through electrochemical deposition, with zinc evenly deposited onto the three-dimensional porous nickel foam structure, exhibiting strong adhesion.

To demonstrate the temporal evolution and effectiveness of zinc electrodeposition on nickel foam substrates, systematic documentation of morphological transformations throughout different deposition stages establishes the correlation between processing parameters and electrode architecture, as illustrated in Fig. 2.

The morphologies of the Zn serial samples are observed by SEM as showed in Fig. 2a-c. Obviously, the morphology of nickel foam after 1 hour of electrodeposition (Fig. 2(a)), exhibits that there a small amount of zinc was deposited initially at the tips and edges of the nickel foam. Fig. 2(b) shows that after 4 hours of electrodeposition, a large amount of zinc is uniformly deposited on the nickel foam framework, forming a continuous layer that fully covers the surface, demonstrating the effectiveness of the deposition process. Fig. 2(c) presents an SEM image of the 4-hour electrodeposited sample, where the zinc layer is observed to adhere relatively uniformly to the nickel foam surface, forming a comparatively dense coating. This indicates that under optimized electrodeposition conditions, the deposited zinc layer can effectively suppress the formation of large particles, which is beneficial for the subsequent performance of zinc-air batteries.

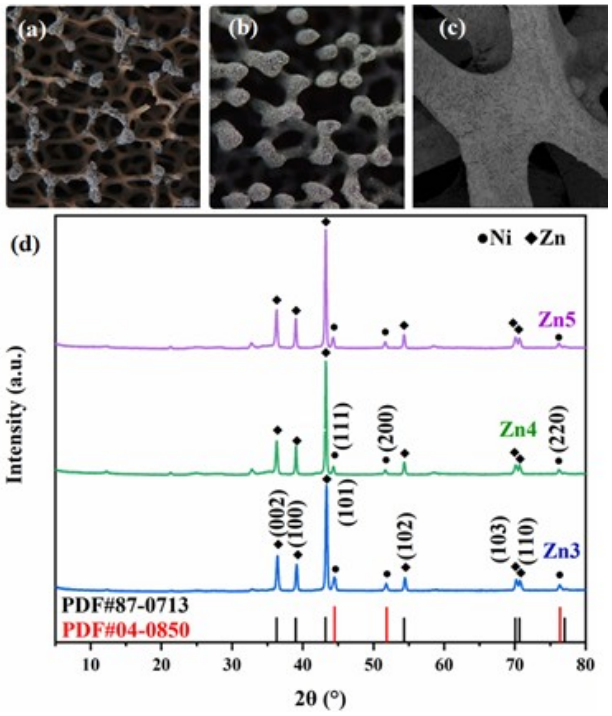

Fig. 2. Results of zinc electrodeposition on nickel foam; (a) Magnified image after 1 hour of electrodeposition, (b) Magnified image after 4 hours of electrodeposition, (c) SEM image of Zn4, (d) XRD patterns of Zn3, Zn4, and Zn5

Fig. 2(d) shows the XRD patterns of the samples with 3 h, 4 h , and 5 h of plating. Characteristic peaks appear at 36.4°, 39.1°, 43.4°, 54.4°, 70.2°, and 70.6°, corresponding to the Zn (002), (100), (101), (102), (103), and (110) planes (PDF#87-0713). Diffraction peaks related to the Ni (111), (200), and (220) planes are also observed at 44.5°, 51.2°, and 76.3° (PDF#04-0850). No characteristic peaks of ZnO are detected, indicating that zinc remains in a good metallic state during preparation.

In addition, the Energy Dispersive Spectroscopy analysis validates the electrodeposition methodology by providing quantitative evidence of zinc distribution uniformity and coverage on the three-dimensional nickel foam substrate. Elemental mapping confirms successful material integration while maintaining the structural integrity of the underlying nickel framework. The spatial analysis reveals comprehensive zinc penetration throughout the internal pore network and complete surface coverage across all accessible substrate areas, establishing the correlation between processing parameters and resulting electrode architecture that influences electrochemical performance, as demonstrated in Fig. 3.

Fig. 3 shows the EDS elemental distribution maps of the 4-hours electrodeposited sample. Fig. 3(a) is an overlay of

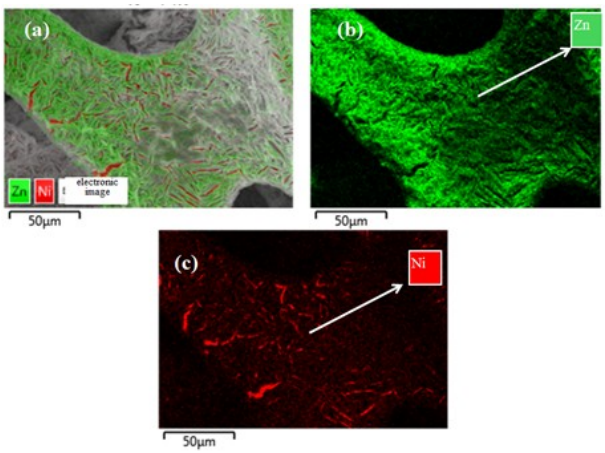

Fig. 3. EDS image of sample electrodeposited for 4 hours; (a) EDS overlay image, (b) EDS map of zinc, (c) EDS map of nickel

the SEM morphology and elemental maps. Fig. 3(b) shows the distribution of zinc, indicating a uniform distribution over the nickel foam framework. Fig. 3(c) presents the distribution of nickel, mainly concentrated in the substrate framework. Fig. 3 discloses that zinc has been successfully deposited onto the nickel foam surface with a uniform distribution.

Furthermore, the energy-dispersive X-ray spectroscopy analysis establishes quantitative baselines for the Zn4 sample by determining mass fractions of the electrodeposited layer. The technique quantifies zinc and nickel mass fractions, enabling precise evaluation of electrodeposition effectiveness, as illustrated in Table 1.

Table 1. Mass fractions of elements in Zn4

Total distribution map of spectrograms			
Element	Signal type	Wt%	Wt% Sigma
Ni	EDS	15.99	0.12
Zn	EDS	84.01	0.12
Total		100.00	

The quantitative elemental analysis presented in Table 1 provides crucial validation of the electrodeposition methodology and offers significant insights into the composite electrode architecture achieved in the Zn4 sample. The EDS results reveal a well-balanced composition with zinc constituting 84.01% and nickel comprising 15.99% of the total mass fraction, demonstrating successful zinc deposition while maintaining substantial nickel foam substrate integrity. The relatively high zinc content of 84.01% indicates that the electrodeposition process achieved substantial zinc loading on the nickel foam substrate, which is essential for maximizing the active material content and,

consequently, the energy storage capacity of the electrode. This loading level suggests optimal utilization of the three-dimensional nickel framework while avoiding excessive zinc accumulation that could compromise the structural advantages of the foam architecture. In addition, the retained nickel fraction of 15.99% is particularly significant from both structural and electrochemical perspectives. This proportion ensures that the nickel foam maintains its mechanical integrity and continues to function as an effective current collector throughout the electrode volume.

Moreover, transmission electron microscopy analysis was utilized to verify the structure and interface quality by resolving the zinc coating at nanoscale resolution in Fig. 4. Concretely, Figs. 4(a)-(b) show TEM images of Zn4, which exhibits a lamellar structure. In Fig. 4(c), the lattice spacings of 0.250 nm and 0.204 nm correspond to the Zn(002) and Ni(111) planes, respectively, indicating that Zn was successfully electroplated onto the Ni substrate, consistent with the XRD and EDS results.

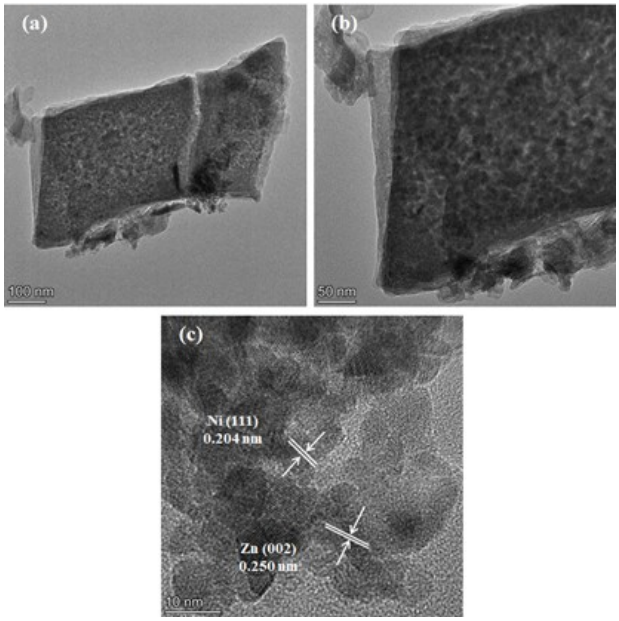

Fig. 4. TEM images of sample electrodeposited for 4 hours and its interplanar spacing; (a)-(b) TEM images of zinc in Zn4, (c) HRTEM image of Zn4.

Figs. 4(a)-(b) show TEM images of Zn4, which exhibits a lamellar structure. In Fig. 4(c), the lattice spacings of 0.250 nm and 0.204 nm correspond to the Zn (002) and Ni (111) planes, respectively, indicating that Zn was successfully electroplated onto the Ni substrate, consistent with the XRD and EDS results.

To assess surface composition and chemical states with the aim of verifying coating quality and establishing a baseline for structure-property correlation, comprehensive high-resolution X-ray photoelectron spectroscopy (XPS) was conducted on the zinc-coated nickel foam, as detailed in Fig. 5.

Fig. 5(a) presents the high-resolution Zn2 p spectra, where Zn3, Zn4, and Zn5 exhibit characteristic peaks near 1022.4 eV and 1045.4 eV , corresponding to $Zn2p_{3/2}$ and $Zn2p_{1/2}$, respectively, indicating that zinc is in the zero-valent state. In Fig. 5(b), the high-resolution O 1s spectra shows characteristic peaks near 531.8 eV for Zn3, Zn4, and Zn5 , corresponding to adsorbed oxygen, further suggesting that zinc remains in a good metallic state during preparation.

3.2. Influence of Deposition Time on Electrochemical Performance and Mechanism Analysis

To systematically investigate the effect of electrodeposition time on zinc loading and electrode structure, the mass of all samples before and after electrodeposition was measured, as shown in Table S1. Additionally, the thickness of the electrodeposited samples was measured, as illustrated in Figure S1. In Table S1, the average thicknesses of the samples were calculated to be 0.8 mm, 0.93 mm, and 1.0 mm , respectively. These results indicate a monotonic increase in both the mass and thickness of the samples with increasing electrodeposition time, suggesting that longer deposition times facilitate the deposition of more zinc onto the nickel foam substrate, thereby enhancing the zinc loading and electrode volume.

Fig. 6 shows the impedance curves of the three samples in a 6 mol/LKOH solution at room temperature. The corrosion of the electrode in the electrolyte is divided into two parts. The high-frequency region corresponds to the loss of electrons from zinc, forming $ZnO_2{}^{2-}$ or $Zn(OH)4^{2-}$, while the low-frequency region represents the diffusion of $ZnO_2{}^{2-}$ or $Zn(OH)4^{2-}$ from the electrode surface into the electrolyte solution. The EIS results indicate that all three samples exhibit similar charge transfer impedances, but Zn4 shows the lowest internal resistance (0.55Ω), suggesting better electrochemical kinetics.

Performance evaluation of the zinc-air batteries encompassed two aspects: open-circuit voltage and load performance. First, the open-circuit voltage variations of StZnB, Zn3B, Zn4B, and Zn5B were measured over 6 hours using an open-circuit test. A data logger was connected directly to the two terminals of the tested batteries to record voltage in real time and transmit the data to a computer for processing and plotting. The specific testing scheme and implementation are shown in Fig. S2.

The open-circuit voltage test scheme and setup are

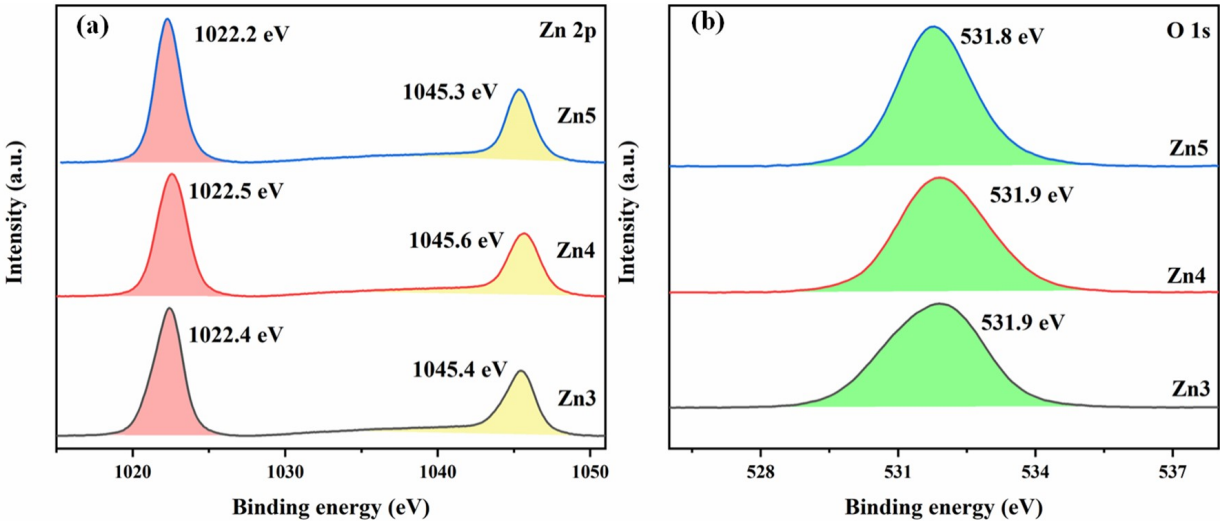

Fig. 5. XPS spectra of samples; (a) High-resolution Zn2p spectra, (b) High-resolution O 1s spectra.

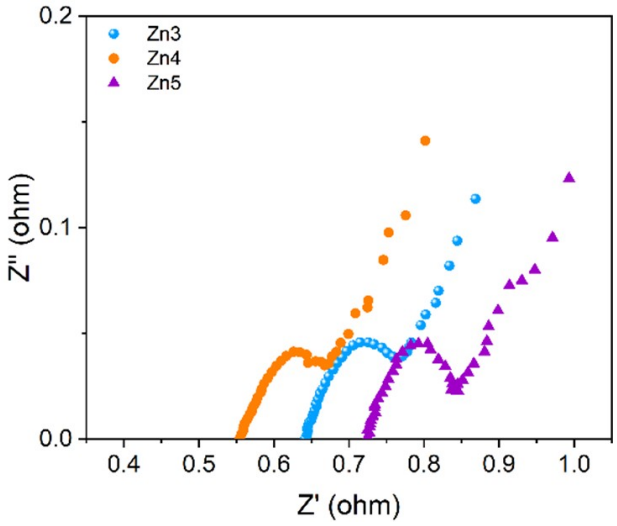

Fig. 6. EIS spectra of the samples.

shown in Figs. S2(a) and S2(b). Subsequently, by connecting the tested batteries to an LED load, the variations in load voltage and load current over 6 hours were measured. The data logger recorded voltage and current separately and plotted the corresponding curves. The load test scheme and setup are shown in Figs. S2(c) and S2(d).

After each battery group was tested, the datasets were gathered, organized, and subjected to routine post-processing to improve clarity and interpretability. Records were checked for consistency, artifacts mitigated, and traces formatted uniformly. From these harmonized data, performance-comparison curves were generated to summarize outcomes and highlight trends, as shown in Fig. 7.

The test results are shown in Figs. 7(a)-(c). As seen in Fig. 7(a), the initial open-circuit voltages of all tested batteries exceed 1.37 V , among which Zn4 B exhibits the highest value at 1.396 V, while the pure zinc plate battery StZnB shows a relatively lower open-circuit voltage. After 6 hours, Zn3 B shows the most pronounced decrease in open-circuit voltage, which can be attributed to that Zn3 sample has a smaller amount of deposited zinc. Spontaneous anode reactions increase internal resistance, leading to a significant drop in open-circuit voltage. From the load voltage results in Fig. 7(b), all batteries exhibit a noticeable drop in initial voltage upon loading; however, Zn4 B maintains the highest voltage, and after 6 hours it still shows a clear advantage, with an average load voltage of 1.17 V . This may be attributed to the favorable electrodeposition in Zn4B: a uniformly distributed zinc layer without obvious dendrite formation. In contrast, Zn3 B may suffer from insufficient deposited zinc, accelerating reactions that further increase internal resistance and reduce output voltage. The load current results in Fig. 7(c) indicate that Zn5 B has the largest initial current, approximately 5.7 mA , however the current decreases sharply within the first hour. This may stem from the large amount of zinc deposited on the Zn5 surface; due to non-uniform deposition, dendrites may form internally during operation, hindering further reactions, increasing internal resistance, and ultimately causing the current to decline.

3.3. Correlation Between Micromorphology and Performance

Scanning electron microscopy analysis assesses surface morphology and coating uniformity through secondary-

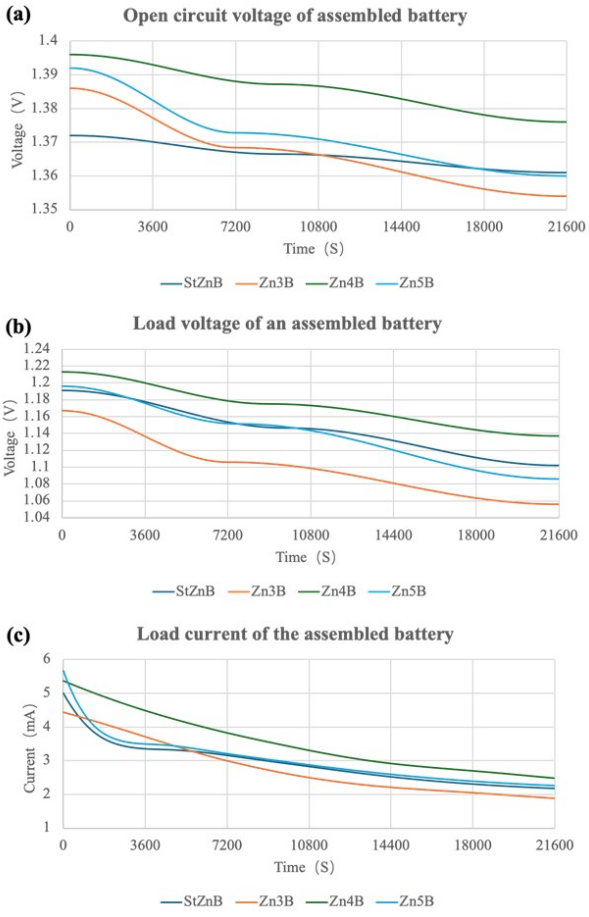

Fig. 7. Battery performance test results; (a) Open-circuit voltage of assembled batteries, (b) Load voltage of assembled batteries, (c) Load current of assembled batteries

electron imaging at multiple magnifications. Low-magnification views reveal pore architecture while high-magnification imaging characterizes grain features. Tilted and cross-sectional observations of ligament and junction regions evaluate zinc coverage continuity, thickness uniformity, and adhesion quality by identifying potential cracks, gaps, or delamination, as shown in Fig. 8.

Fig. 8 shows the surface micro morphologies of Zn3, Zn4, and Zn5 with different electrodeposition times, clearly revealing how deposition affects the performance of zinc-air batteries. Figs. 8(a)-(c) depict the surface morphology of Zn3 . Owing to the insufficient deposition time, a loose flocculent structure forms on the surface with limited reactive area, which may cause pronounced decreases in load voltage and current after cell assembly due to inadequate anode active material. Figs. 8(d)-(f) show the surface morphology of Zn4. With a moderate deposition time, a

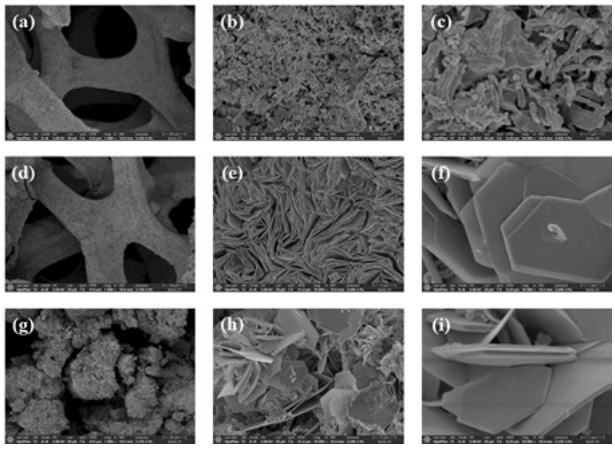

Fig. 8. SEM images of sample; (a)-(c) SEM images of Zn3 at $1,000 \times 10,000\times$, and $50,000\times$, (d)-(f) SEM images of Zn4 at $1,000 \times 10,000\times$, and $50,000\times$, (g)-(j) SEM images of Zn5 at $1,000 \times 10,000\times$, and $50,000\times$

relatively uniform lamellar structure forms, which enlarges the electrochemical reaction area and provides sufficient active material, thereby yielding better stability in both load voltage and current. Figs. 8(g)-(j) present the surface morphology of Zn5. Due to the longer deposition time, more blocky aggregated structures form; these irregular blocks may impede ion transport during operation, hinder further electrochemical reactions, and thus degrade load voltage and current performance.

4. Conclusion

This work systematically elucidates how electrodeposition time influences the performance and underlying mechanism of zinc anodes on nickel foam. The experimental results reveal that the 4 hours deposited sample achieves the optimal balance between zinc loading (84.01wt%) and deposition uniformity, delivering the best overall performance with an average load voltage of 1.17 V , load current of 3.52 mA , and a 21% improvement over purezinc anodes. The superior performance arises from two synergistic factors: i) sufficient zinc deposition ensures ample reactive material, ii)moderate plating time promotes uniform zinc layers that suppress dendrite growth and optimize the reaction environment. We establish a multi-level "deposition time-zinc loading-microstructure-electrochemical performance" correlation model, providing a clear process window for zinc-air anode fabrication (recommended 4 h plating) and theoretical guidance, as well as methodological reference for other metal-air battery electrodes. Future work will focus on enhancing current output and further improving overall performance via electrolyte formulation

optimization and stresscontrol strategies.

Acknowledgements

This research has received funding and support from the Silpakorn University Research, Innovation, and Creative Fund.

References

[1] H. S. Hayajneh and X. Zhang, (2020) *"Logistics Design for Mobile Battery Energy Storage Systems"* **Energies** ***13***(5): 1157. DOI: 10.3390/en13051157.

[2] Z. Zhu, T. Jiang, M. Ali, Y. Meng, Y. Jin, Y. Cui, and W. Chen, (2022) *"Rechargeable Batteries for Grid Scale Energy Storage"* **Chemical Reviews** ***122***(22): 16610–16751. DOI: 10.1021/acs.chemrev.2c00289.

[3] R.-B. Huang, M.-Y. Wang, J.-F. Xiong, H. Zhang, J.-H. Tian, and J.-F. Li, (2025) *"Anode optimization strategies for zinc–air batteries"* **eScience** ***5***(3): 100309. DOI: 10.1016/j.esci.2024.100309.

[4] J. Fu, Z. P. Cano, M. G. Park, A. Yu, M. Fowler, and Z. Chen, (2017) *"Electrically Rechargeable Zinc-Air Batteries: Progress, Challenges, and Perspectives"* **Advanced Materials** ***29***(7): 1604685. DOI: 10.1002/adma.201604685.

[5] R. Khezri, S. Rezaei Motlagh, M. Etesami, A. A. Mohamad, F. Mahlendorf, A. Somwangthanaroj, and S. Kheawhom, (2022) *"Stabilizing zinc anodes for different configurations of rechargeable zinc-air batteries"* **Chemical Engineering Journal** ***449***: DOI: 10.1016/j.cej.2022.137796.

[6] J. B. Goodenough and K.-S. Park, (2013) *"The Li-Ion Rechargeable Battery: A Perspective"* **Journal of the American Chemical Society** ***135***(4): 1167–1176. DOI: 10.1021/ja3091438.

[7] J. Zhang, Q. Zhou, Y. Tang, L. Zhang, and Y. Li, (2019) *"Zinc–air batteries: are they ready for prime time?"* **Chemical Science** ***10***(39): 8924–8929. DOI: 10.1039/C9SC04221K.

[8] N. Nitta, F. Wu, J. T. Lee, and G. Yushin, (2015) *"Li-ion battery materials: present and future"* **Materials Today** ***18***(5): 252–264. DOI: 10.1016/j.mattod.2014.10.040.

[9] M. Winter, B. Barnett, and K. Xu, (2018) *"Before Li Ion Batteries"* **Chemical Reviews** ***118***(23): 11433–11456. DOI: 10.1021/acs.chemrev.8b00422.

[10] M. Li, J. Lu, Z. Chen, and K. Amine, (2018) *"30 Years of Lithium-Ion Batteries"* **Advanced Materials** ***30***(33): 1800561. DOI: 10.1002/adma.201800561.

[11] P. Gu, M. Zheng, Q. Zhao, X. Xiao, H. Xue, and H. Pang, (2017) *"Rechargeable zinc–air batteries: a promising way to green energy"* **Journal of Materials Chemistry A** ***5***(17): 7651–7666. DOI: 10.1039/C7TA01693J.

[12] C. Shunhong, S. Pullteap, and T. Mao, (2024) *"Research Progress and Future Expectations in Anode of Secondary Zinc-Air Batteries: A Review"* **Applied Science and Engineering Progress**: DOI: 10.14416/j.asep.2024.06.006.

[13] L. Li, Y. C. A. Tsang, D. Xiao, G. Zhu, C. Zhi, and Q. Chen, (2022) *"Phase-transition tailored nanoporous zinc metal electrodes for rechargeable alkaline zinc-nickel oxide hydroxide and zinc-air batteries"* **Nature Communications** ***13***(1): 2870. DOI: 10.1038/s41467-022-30616-w.

[14] K. Harting, U. Kunz, and T. Turek, (2012) *"Zinc-air Batteries: Prospects and Challenges for Future Improvement"* **Zeitschrift für Physikalische Chemie** ***226***(2): 151–166. DOI: 10.1524/zpch.2012.0152.

[15] X. Chen, Z. Zhou, H. E. Karahan, Q. Shao, L. Wei, and Y. Chen, (2018) *"Recent Advances in Materials and Design of Electrochemically Rechargeable Zinc–Air Batteries"* **Small** ***14***(44): 1801929. DOI: 10.1002/smll.201801929.

[16] O. Haas, F. Holzer, K. Müller, and S. Müller. "Metal/air batteries: the zinc/air case". en. In: *Handbook of Fuel Cells*. 2010. DOI: 10.1002/9780470974001.f104022.

[17] E. Davari, A. D. Johnson, A. Mittal, M. Xiong, and D. G. Ivey, (2016) *"Manganese-cobalt mixed oxide film as a bifunctional catalyst for rechargeable zinc-air batteries"* **Electrochimica Acta** ***211***: 735–743. DOI: 10.1016/j.electacta.2016.06.085.

[18] D. Liu, Y. Tong, X. Yan, J. Liang, and S. X. Dou, (2019) *"Recent Advances in Carbon-Based Bifunctional Oxygen Catalysts for Zinc-Air Batteries"* **Batteries & Supercaps** ***2***(9): 743–765. DOI: 10.1002/batt.201900052.

[19] M. Wu, G. Zhang, Y. Hu, J. Wang, T. Sun, T. Regier, J. Qiao, and S. Sun, (2021) *"Graphitic-shell encapsulated FeNi alloy/nitride nanocrystals on biomass-derived N-doped carbon as an efficient electrocatalyst for rechargeable Zn-air battery"* **Carbon Energy** ***3***(1): 176–187. DOI: 10.1002/cey2.52.

[20] J. Ding, P. Wang, S. Ji, H. Wang, V. Linkov, and R. Wang, (2019) *"N-doped mesoporous FeNx/carbon as ORR and OER bifunctional electrocatalyst for rechargeable zinc-air batteries"* **Electrochimica Acta** ***296***: 653–661. DOI: 10.1016/j.electacta.2018.11.105.

[21] R. Khezri, S. R. Motlagh, M. Etesami, P. Pakawanit, S. Olaru, A. Somwangthanaroj, and S. Kheawhom, (2024) *"Balancing current density and electrolyte flow for improved zinc-air battery cyclability"* **Applied Energy *376***: 124239. DOI: 10.1016/j.apenergy.2024.124239.

[22] T. Placke, R. Kloepsch, S. Dühnen, and M. Winter, (2017) *"Lithium ion, lithium metal, and alternative rechargeable battery technologies: the odyssey for high energy density"* **Journal of Solid State Electrochemistry *21***(7): 1939–1964. DOI: 10.1007/s10008-017-3610-7.

[23] J. F. Parker, C. N. Chervin, I. R. Pala, M. Machler, M. F. Burz, J. W. Long, and D. R. Rolison, (2017) *"Rechargeable nickel–3D zinc batteries: An energy-dense, safer alternative to lithium-ion"* **Science**: DOI: 10.1126/science.aak9991.

[24] M. Wang, F. Zhang, C.-S. Lee, and Y. Tang, (2017) *"Low-Cost Metallic Anode Materials for High Performance Rechargeable Batteries"* **Advanced Energy Materials *7***(23): 1700536. DOI: 10.1002/aenm.201700536.

[25] J. Yi, P. Liang, X. Liu, K. Wu, Y. Liu, Y. Wang, Y. Xia, and J. Zhang, (2018) *"Challenges, mitigation strategies and perspectives in development of zinc-electrode materials and fabrication for rechargeable zinc–air batteries"* **Energy & Environmental Science *11***(11): 3075–3095. DOI: 10.1039/C8EE01991F.

[26] J. F. Parker, J. S. Ko, D. R. Rolison, and J. W. Long, (2018) *"Translating Materials-Level Performance into Device-Relevant Metrics for Zinc-Based Batteries"* **Joule *2***(12): 2519–2527. DOI: 10.1016/j.joule.2018.11.007.

[27] D. E. Turney, J. W. Gallaway, G. G. Yadav, R. Ramirez, M. Nyce, S. Banerjee, Y.-c. K. Chen-Wiegart, J. Wang, M. J. D'Ambrose, S. Kolhekar, J. Huang, and X. Wei, (2017) *"Rechargeable Zinc Alkaline Anodes for Long-Cycle Energy Storage"* **Chemistry of Materials 29**(11): 4819–4832. DOI: 10.1021/acs.chemmater.7b00754.

[28] J. Pan, Y. Y. Xu, H. Yang, Z. Dong, H. Liu, and B. Y. Xia, (2018) *"Advanced Architectures and Relatives of Air Electrodes in Zn–Air Batteries"* **Advanced Science *5***(4): 1700691. DOI: 10.1002/advs.201700691.

[29] K. Wang, Y. Zuo, P. Pei, X. Liu, M. Wei, Y. Xiao, J. Xiong, and P. Zhang, (2021) *"Zn–Ni reaction in the alkaline zinc-air battery using a nickel-supported air electrode"* **Materials Today Energy *21***: 100823. DOI: 10.1016/j.mtener.2021.100823.

[30] K. Wang, P. Pei, Y. Wang, C. Liao, W. Wang, and S. Huang, (2018) *"Advanced rechargeable zinc-air battery with parameter optimization"* **Applied Energy 225**: 848–856. DOI: 10.1016/j.apenergy.2018.05.071.

[31] Y.-P. Deng, Y. Jiang, R. Liang, S.-J. Zhang, D. Luo, Y. Hu, X. Wang, J.-T. Li, A. Yu, and Z. Chen, (2020) *"Dynamic electrocatalyst with current-driven oxyhydroxide shell for rechargeable zinc-air battery"* **Nature Communications *11***(1): 1952. DOI: 10.1038/s41467-020-15853-1.

[32] H. Pan, Y. Shao, P. Yan, Y. Cheng, K. S. Han, Z. Nie, C. Wang, J. Yang, X. Li, P. Bhattacharya, K. T. Mueller, and J. Liu, (2016) *"Reversible aqueous zinc/manganese oxide energy storage from conversion reactions"* **Nature Energy *1***(5): 16039. DOI: 10.1038/nenergy.2016.39.